Appl Magn Reson
DOI 10.1007/s00723-015-0717-9

Applied
Magnetic Resonance

Dual Localization of Paramagnetic Probe Molecules in Smectic Liquid Crystals

Daria A. Pomogailo[1] · Natalia A. Chumakova[1] · Sergei M. Pestov[2] · Andrey Kh. Vorobiev[1]

Received: 18 November 2014 / Revised: 19 May 2015

Abstract Molecular localization of nitroxide stable radicals in three smectic liquid crystals (4-*n*-octyl-4′-cyanobiphenyl (8CB), *p*-hexyloxyphenyl ester of *p*-octyloxybenzoic acid (HOPOOB) and *p*-hexyloxyphenyl ester of *p*-decyloxybenzoic acid (HOPDOB)) was analyzed by means of numerical simulation of electron paramagnetic resonance spectra. It was shown that admixture molecule can be localized in the structure of smectic LC in several different ways. The studied nitroxide molecules demonstrated dual localization in HOPOOB and HOPDOB but unique localization in 8CB. The radical molecules with different localization are distinguished by the values of rotation diffusion coefficients and by the direction of the main rotation axis.

Electronic supplementary material The online version of this article (doi:10.1007/s00723-015-0717-9) contains supplementary material, which is available to authorized users.

✉ Daria A. Pomogailo
texafirin@yandex.ru

Natalia A. Chumakova
harmonic2011@yandex.ru

Sergei M. Pestov
pestovsm@yandex.ru

Andrey Kh. Vorobiev
a.kh.vorobiev@gmail.com

[1] Department of Chemistry, M.V. Lomonosov Moscow State University, Leninskie Gory 3-1, Moscow 119991, Russian Federation

[2] Lomonosov Moscow State University of Fine Chemical Technologies, Prospect Vernadskogo 86, Moscow 119571, Russian Federation

Published online: 13 August 2015

1 Introduction

The molecular probe methods are commonly used for determination of structural and dynamical characteristics of liquid crystalline materials. The probe techniques are based on measurements of characteristics of admixture molecules embedded into studied LC medium. Different properties of molecular probe can be monitored. For example, linear dichroism or fluorescence polarization is measured in the case of optical probe techniques [1–9]. The electron paramagnetic resonance (EPR) spectra of paramagnetic molecular probes are used as a source of information in a spin probe technique [10–14]. In the cases of spatially inhomogeneous materials, spin probe technique gives the direct information concerning the properties of different phases and substructures of medium. The paramagnetic probe molecules with different localization in heterogeneous medium demonstrate the different characteristics and generate the EPR spectra, which are combination of two or more individual spectra. Analysis of such composite spectra has revealed the characteristics of polymer and liquid crystalline microphases in polymer-dispersed liquid crystal materials [15], features of liquid crystalline and liquid-ordered phases in membrane vesicles [16], properties of different sites in proteins (see, for example, [17]), etc. On the other hand, the study of smectic liquid crystals by means of spin probe technique was based until now on the assumption that all probe molecules are identical in their orientational and dynamical characteristics (see, for instance, [18–20]). Smectic mesophases are clearly inhomogeneous media as they are composed of layers and interlayer space. The probe molecules localized in different points of such a medium have to differ in the dynamical and orientational characteristics. However, until today there has been no publication, which demonstrates the various ways or modes of localization of probe molecules in smectics. Thus, the aim of present work is to detect the spatial variation of properties of smectics by means of spin probe technique.

Earlier we have shown [21] that stable nitroxide radicals with paramagnetic moiety in the central core reflect orientation of liquid crystals more adequately in comparison with standard spin probes of piperidine series. The main fragment of these radicals is the phenylbenzoate moiety (Fig. 1). It is known that phenylbenzoate is the structural unit of few smectic liquid crystals. In our investigation, we have chosen the liquid crystal and probe molecules containing the same phenylbenzoate fragment in the hope to observe specific localization of the probe molecules and to obtain from EPR spectra more detailed structural information. It is known that both macroscopic orientational order and molecular rotational mobility influence appreciably on EPR spectral shape of nitroxide probe [11, 18, 22]. At present, the orientation order is described mostly by the mean field potential [12, 23]. Unfortunately, this approach leads to ambiguous results, which demonstrate the interdependence of orientational and rotational parameters [24]. To exclude this trouble, in the present work, we studied the unordered liquid crystalline media. This experimental approach allows extracting characteristics of rotation mobility of probe molecules solely, without complications caused by macroscopic order of medium. It is possible in the case of smectic mesophases, as magnetic field of EPR spectrometer does not induce the macroscopic order of the medium.

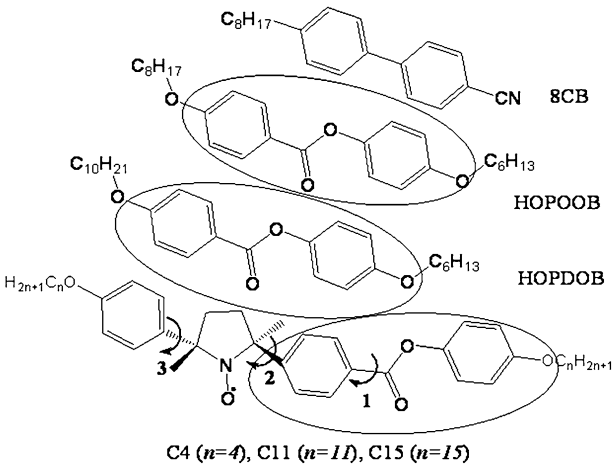

Fig. 1 Molecular structures of liquid crystalline compounds and spin probes. The identical fragments of spin probes and liquid crystals HOPOOB and HOPDOB are marked by *circles*. Intramolecular rotations around bonds *1*, *2* and *3* are marked by *arrows* (see the text)

2 Experiment Details

2.1 Substances

Liquid crystal 8CB (4-*n*-octyl-4′-cyanobiphenyl) by Aldrich was used without further purification. Polymesomorphic HOPDOB (p-hexyloxyphenyl ester of p-decyloxybenzoic acid) and HOPOOB (*p*-hexyloxyphenyl ester of *p*-octyloxybenzoic acid) were produced by RIAP (Kiev) and were purified by recrystallization from ethyl acetate. These molecular structures are shown in Fig. 1. The liquid crystalline substances have nematic and smectic mesophases in the following temperature ranges [T, K]:

Cr-(294,2)-SmA-(305,7)-N-(313,2)-Iso for 8CB [25];

Cr-(329,1)-SmC-(338,6)-N-(362,4)-Iso for HOPOOB [26, 27];

Cr-(335,6)-(SmE-(311,1)-SmB-(317,6))-SmC-(350,6)-SmA-(356,4)-N-(362,0)-Iso for HOPDOB [27, 28].

LC HOPDOB demonstrates the monotropic smectic E and B phases and enantiotropic smectic C and A phases [28–30]. However, unstable E and B phases were not studied in the present work [28–30].

The nitroxide radicals with general formula 2,5-dimethyl-2-alkoxyphenyl-5-[4-(4-alkoxybenzenecarbonyloxy)phenyl] pyrrolidine-1-oxide (Fig. 1) were used as spin probes. The structure of the central fragment of the radicals is shown in Fig. 1. These substances were kindly granted by Prof. R. Tamura (Kyoto University). The synthesis of the radicals is described in detail in [31, 32].

2.2 Sample Preparation

The solutions of spin probes in liquid crystals with concentration of about 10^{-3} mol/L were placed into the quartz ampoules (inner diameter $\sim$3 mm, sample height $\sim$10 mm) and were degassed at pressure of 10^{-3} Torr for 2 h. The frozen disordered samples were prepared by heating of solutions above the LC clearing point and following rapid cooling down to 77 K by immersion in liquid nitrogen. To obtain the unordered smectic sample, the cooling from isotropic state to the temperature of existence of mesophase was carried out without magnetic field. The absence of angular dependence of EPR spectra was verified. The additional verifications were obtained by the following experiments. The sample at the temperature of smectic mesophase was put in the resonator of spectrometer and EPR spectrum was recorded. Then, the magnetic field was fixed in a certain value and the signal amplitude at this field was recorded as time dependent during the sudden turn of the sample. The kinetic curves recorded during such experiments have confirmed the absence of reorientations of smectics in the magnetic field of EPR spectrometer.

2.3 EPR Spectra Recording

X-band EPR spectra were recorded with EPR spectrometers "Varian E3" and "Bruker EMXplus". For recording of the spectrum at the mesophase temperature, the ampoule was placed into EPR Dewar tube with air flow of required temperature. The temperature was controlled with accuracy of $\pm$0.5 °C. It was found experimentally that the sample reaches the temperature after 3 min.

Recording of spectra for frozen samples was carried out in a Dewar flask, filled with liquid methane ($T = 113$ K).

2.4 EPR Spectra Simulation

Extraction of dynamical characteristics of nitroxide molecules was performed by numerical simulation of EPR spectra. The values of required parameters were obtained by means of minimization of the discrepancy between the calculated and experimental spectra by nonlinear least-squares fitting procedures [36]. The results of simulation were considered as acceptable when the discrepancy between experimental and simulated spectra was lower than the noise level of spectra recording.

In present work, two kinds of spectra simulations were carried out. The simulations of the spectra for frozen solutions (rigid-limit spectra) were used for determination of magnetic parameters of probes. Such simulations were performed using a home-made program described in detail in [13] and available at [33]. The obtained values of spin-Hamiltonian parameters were used then in course of spectra simulation for probes in smectic phases. These simulations were accomplished within the slow-motion regime using the stochastic Liouville equation (SLE) and the model of anisotropic Brownian diffusion [23]. The varied parameters in course of these simulations were coefficients of rotation diffusion of radicals and angles

describing the directions of rotational axes of paramagnetic particles. In the course of simulation of both rigid-limit and high-temperature spectra, the width of individual resonance line was calculated as convolution of Gaussian and Lorentzian functions. The main axes of both Gauss and Lorentz linewidth tensors coincided with the main axes of g-tensor.

The results of EPR spectra simulation in rigid limit and mesophase are presented in Fig. 2a, b as examples.

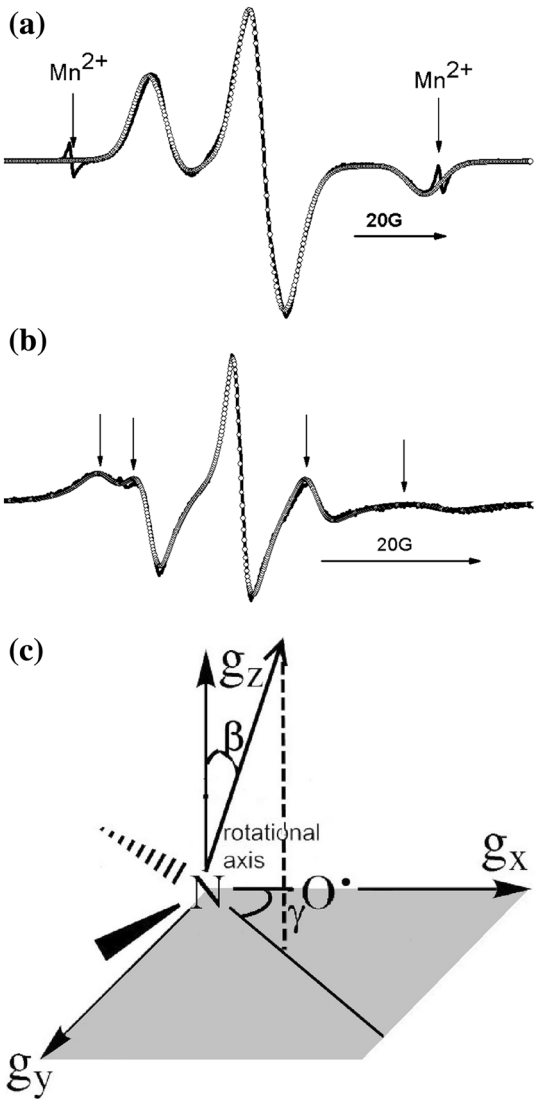

Fig. 2 EPR spectra of radical C4 in smectic liquid crystal 8CB, recorded in supercooled state at temperature 113 K (**a**) and in smectic mesophase state at 304 K (**b**), and the results of their simulation (experimental spectra—*solid lines*, calculated spectra—*open circles*); g-tensor coordinate frame of nitroxide moiety (**c**)

2.5 Calculation of the Inertia Tensors of Probe Molecules

The main values and principal axes of inertia tensor for probe molecules were calculated using molecular geometry optimized by DFT calculation. The geometry optimizations were carried out using program package ORCA in model B3LYP/6-31 g(d,p) for continuum medium (toluene at temperature 293 K). Calculations of optimal geometry were carried out for probe molecules with different length and conformation of side alkyl substitutes. It was found out that geometry of the core fragment is almost independent both of the length and conformation of side substitutes. For this reason, calculations of inertia tensor were carried out excluding the substitutes.

Cartesian coordinates for the optimal geometry of the central fragment are presented in Table S1 of Supporting Information. To take into account possible intramolecular rotations inside core fragments of probe, the energy barriers for three intramolecular rotations marked by arrows in Fig. 1 were estimated. For each rotation, the optimization of geometry and determination of full energy of the system was performed with step of 10° (see Supporting Information). Figures S2a, b, c in Supporting Information point to the fact that rotation around all three bonds is restricted. So all rotational isomers contribute to the inertia tensor of the molecule. To examine the influence of the intramolecular rotations on the inertia properties, we have calculated the averaged inertia tensor for every rotation separately. For this purpose, the averaging was made with Boltzmann contribution of each rotational conformer. The result characteristics of inertia tensors for three possible intramolecular rotations are presented in Table 1. It is seen that intramolecular rotations have no dramatic effect on both main values of inertia moments and direction of the main inertia axis.

The data presented in Table 1 demonstrate also that inertia tensor of considered probe molecules is approximately axial. The angles β, γ define the direction of the main rotational axis in the magnetic coordinate frame of nitroxide molecule, which is the g-tensor principal axes. Thus, the direction of the main inertia axis for the central fragment of probe molecules is defined approximately by values $\beta \sim 50°$, $\gamma \sim 84°$ in g-tensor frame.

3 Results and Discussion

The spectra of radical probes C4, C11 and C15 (Fig. 1) in liquid crystals 8CB, HOPOOB and HOPDOB (Fig. 1) were both recorded at the temperatures of existence of smectic mesophases and in supercooled state at 113 K. The spectra of C4 in 8CB at 304 and 113 K are presented in Fig. 2 as examples.

Table 1 Characteristics of inertia tensors for three possible inner rotations

	ΔE_{rot} (kJ/mol)	I_x, r.u.	I_y, r.u.	I_z, r.u.	β, γ
Optimal geometry		12,850	12,712	883	52°, 84°
Rotation 1	3.6	12,778	12,645	1008	48°, 88°
Rotation 2	8.7	14,296	13,986	1229	50°, 80°
Rotation 3	7.5	13,548	13,406	933	51°, 85°

The rigid-limit spectra recorded at 113 K (Fig. 2a) were typical for motionless nitroxide radicals. The spectra are broadened because of the anisotropy of g-value and hyperfine interaction. These spectra were used for determination of the magnetic parameters of the radicals in studied matrices. It was found that these spectra are simulated within the level of recording accuracy in the assumption that principal axes of g-tensor coincide with the axes of the HFS tensor that is typical for nitroxides. The components of the g-tensor and hyperfine tensor for all examined probe-matrix systems are the same within errors of determination: $g_x = 2.0089 \pm 0.0002$, $g_y = 2.0064 \pm 0.0002$, $g_z = 2.0024 \pm 0.0002$, $A_x = 0.5 \pm 0.05$ mT, $A_y = 0.34 \pm 0.05$ mT, $A_z = 3.236 \pm 0.010$ mT.

The spectra recorded at temperature of smectic mesophase demonstrate typical slow-motion shape (Fig. 2b). The relatively rapid rotation around one axis averages partially the magnetic anisotropy and leads to uniaxial magnetic characteristics of rotating radical [34, 35]. This axiality manifests itself in the splitting of outermost components of EPR spectrum marked on Fig. 2b by arrows. The positions of these components reflect the direction of main rotational axis relative to the g-tensor frame of nitroxide moiety (Fig. 2c). Thus, the numerical simulation of such spectra provides values of the rotation diffusion coefficients and Euler angles defining the direction of rotation axis of probe molecule. Despite the relatively small temperature ranges of mesophase existence in liquid crystals under consideration there is noticeable temperature dependence of EPR spectra. Spectra of radical C4 in liquid crystal HOPDOB are presented in Fig. 5a, b as an illustration. The rotational parameters of the radicals in smectic mesophases of the liquid crystals under consideration were determined by simulation of the EPR spectra recorded in the temperature ranges (297–304) K for 8CB, (330–336) K for HOPOOB and (337–355) K for HOPDOB. It was found that spectra of spin probes C4 and C11 in 8CB are successfully simulated in the assumption that all paramagnetic molecules have identical rotational characteristics. The coefficients of rotation diffusion of radicals C4 and C11 in 8CB and the angles defining direction of rotational axis relative to the g-tensor are presented in Table 2.

One can see from Table 2 that rotation of paramagnetic probe molecules studied is significantly anisotropic. The coefficients of rotation diffusion of the radicals around one molecular axis exceed the coefficients of rotation around perpendicular axes by two orders of magnitude. Direction of the main rotational axis in g-tensor frame is defined by Euler angles β and γ (Fig. 2c). The presented data demonstrate that the direction of the main rotational axis for radicals with both long (C11) and

Table 2 Parameters of rotational mobility of probes C4 and C11 in 8CB

Probe	C4			C11				
T, K	298	301	304	297	299	301	303	304
$Dx = Dy$ (s^{-1})	$<4{\cdot}10^6$			$<4{\cdot}10^6$				
$Dz10^{-8}$ (±5 %)* (s^{-1})	3.4	3.8	4.6	2.8	3.0	3.3	3.4	3.5
$\beta \pm 0.5$ (°)	37	38	38	38	38	38	38	38
$\gamma \pm 0.5$ (°)	90	90	90	90	90	90	90	90

* The accuracy level is presented in brackets

short (C4) alkyl substituents in 8CB is the same and does not depend on temperature. The rotational axis is directed approximately along the central rigid core of the paramagnetic molecule ($\beta \sim 38°$, $\gamma \sim 90°$) but does not coincide with the direction of molecular main inertia axis ($\beta \sim 50°$, $\gamma \sim 84°$). Obviously, this difference is the result of interaction of probe molecule with the LC matrix. Thus, rotation of admixture molecule in the liquid crystalline matrix is not determined by molecular geometry only.

Rotation diffusion coefficients for radical C4 in liquid crystal 8CB insignificantly exceed corresponding values for radical C11. Rotation of paramagnetic molecules with both short and long alkyl substituents accelerates in some degree with temperature increasing. Temperature dependence of rotation diffusion coefficient D_z of the spin probes in 8CB is shown in Fig. 3.

Unlike the systems C4-8CB and C11-8CB, the spectra of spin probes in smectic liquid crystals HOPOOB and HOPDOB cannot be simulated assuming only one mode of rotation of paramagnetic molecules. The spectrum of radical C4 in HOPDOB at temperature 352 K in SmA mesophase is presented in Fig. 4a. The additional components in the low-field and high-field parts of the spectrum are marked by arrows. Numerical simulations can reproduce these components only if coexistence of two types of paramagnetic molecules with different rotational characteristics takes place. This assumption was found to be necessary for simulation of the experimental spectra within the accuracy of recording both in the cases of HOPOOB and HOPDOB media. The results of simulation of the spectra for C4 in HOPDOB and HOPOOB are shown in Fig. 4a, b as the examples. The calculated spectra for probes with different rotational parameters are shown in the figure separately and marked by 2 and 3. Thus, the shape of the EPR spectra showed that in HOPDOB and HOPOOB liquid crystals there are two types of radical probe localizations, which are characterized by different parameters of rotation.

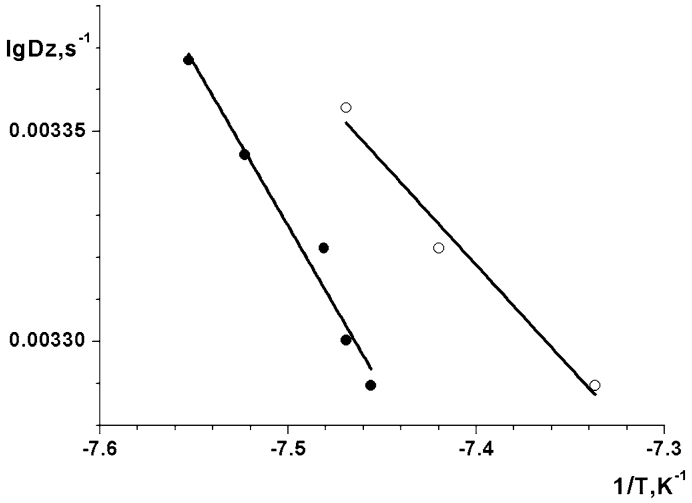

Fig. 3 Temperature dependence of rotation diffusion coefficient D_z for spin probes C4 (*open circles*) and C11 (*closed circles*) in 8CB

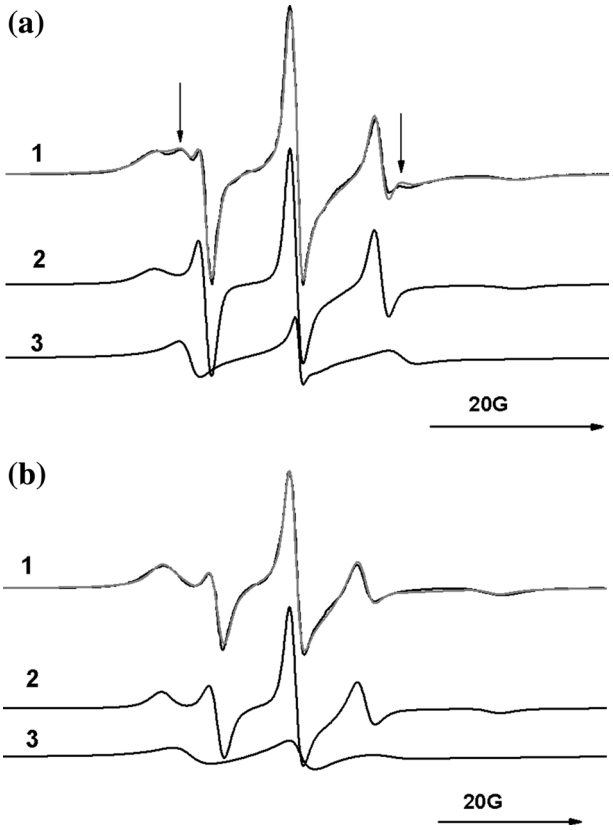

Fig. 4 *1*-Experimental (*black lines*) and simulated (*gray lines*) EPR spectra of radical C4 in HOPDOB at 352 K (**a**) and in HOPOOB at 330 K (**b**); *2* and *3 lines* show spectral contributions of radicals type I and type II, which differ in their rotational characteristics

The rotational parameters of spin probes in HOPOOB and HOPDOB are presented in Tables 3 and 4. One can see that the diffusion coefficients characterizing rotation around the *z*-axis for radicals with different localization differ by an order of magnitude. Below we designate rapidly rotating radicals as particles type I, and slowly rotating ones as particles type II. Contents of radicals I [denote N(I)] and radicals II [N(II)] are shown in Tables 3 and 4. From the data presented in the Tables, it is seen that the contents of radicals I and II are comparable but depend to some degree on the length of alkyl substitutes in paramagnetic molecules. Temperature dependence of contents of radicals I and II is weak and is within the errors of determination.

EPR spectra for radicals C4 in SmA and SmC phases HOPDOB are shown in Fig. 5. One can see that the shape of spectrum depends on the mesophase type significantly. Temperature dependence of rotation diffusion coefficient D_z for radicals C4 and C15 of type II in HOPDOB matrix is shown in Fig. 6. The values of this coefficient lie in the range $(1.9–6.5)\cdot 10^8$ s^{-1} and can be determined quite precisely by the simulation of EPR spectra. On the contrary, the diffusion

Table 3 Parameters of rotational movement of probes C4, C15 in HOPOOB

Probe	C4				C15		
T, K	330	332	334	336	330	332	334
Type I							
N(I) ±2 %	55 %	49 %	48 %	47 %	60 %	59 %	53 %
$Dx(I) = Dy(I)$ (s^{-1})	$<4{\cdot}10^6$				$<4{\cdot}10^6$		
$Dz(I)$ 10^{-9}, (±5 %) (s^{-1})	1.4	1.6	2.2	2.6	1.7	1.6	1.8
$\beta(I)$ ± 0.5 (°)	35	35	35	35	34	35	35
$\gamma(I)$ ± 0.5 (°)	90	90	90	90	90	90	90
Type II							
N(II) ±2 %	45 %	51 %	52 %	53 %	40 %	41 %	47 %
$Dx(II) = Dy(II)$ (s^{-1})	$<4{\cdot}10^6$				$<4{\cdot}10^6$		
$Dz(II)$ 10^{-8} (±5 %) (s^{-1})	1.8	1.6	1.8	1.9	2.0	2.2	2.0
β(II) ± 0.5 (°)	57	60	60	60	60	60	61
γ(II) ± 0.5 (°)	90	90	90	90	90	90	90

coefficients of radicals type I in HOPDOB lie in the interval $(1.5–4.2){\cdot}10^9$ s^{-1} and are determined with considerable uncertainty. Therefore, the temperature dependence of Dz-value for type I radicals is within the error of determination.

The data presented in Tables 2, 3 and 4 show that angles β and γ of probe molecules studied are almost independent of the length of side alkyl substitutes. Therefore, the rotational axes of used probe molecules are defined predominantly by the central molecular fragment.

The direction of the main rotational axis of radicals type I for the systems C4-HOPOOB, C15-HOPOOB and C15-HOPDOB ($\beta \sim 36°$, $\gamma \sim 90°$) coincides with direction of rotational axis of radicals in 8CB. The direction of the rotational axis of radicals type II (β(II) $\sim$ (57–60)°, γ(II) $\sim$ 90°) deviates from the direction of rotation axis for radicals type I. The rotational axes for fast and slowly rotating radicals and inertia axis of central fragment of molecules are shown in Fig. 7.

For the system C4-HOPDOB, the directions of rotational axes for radicals of both types differ to some extent from the directions of rotational axes for other examined systems.

In general, we can state that spin probes in liquid crystalline matrices HOPOOB and HOPDOB have at least two sufficiently different modes of localization. This fact can be explained by the following structural features of spin probes and liquid crystals molecules. The probe molecules and molecules of HOPDOB and HOPOOB contain the same phenylbenzoate fragments, which are marked in Fig. 1 by circles. This similarity makes possible the substitution of LC molecule by probe molecule in the structure of smectic layer. It is known that smectic layers in the case of HOPOOB and HOPDOB are stabilized by intermolecular π-stacking interactions [37, 38]. There are two sites capable of π-stacking in the structure of used probe molecules. They are phenylbenzoate moiety and oxyphenyl group. Perhaps, it is the cause of two different localizations realized for these probe molecules in the smectic

Table 4 Parameters of rotational movement of probes C4, C15 in HOPDOB

Probe	C4								C15							
T, K	SmC				SmA				SmC				SmA			
Phase	337	338	340	348	352	353	354	355	337	340	345	348	352	353	354	355
Type I																
N(I) ± 2 %	41 %	42 %	41 %	46 %	52 %	52 %	55 %	54 %	59 %	58 %	57 %	55 %	59 %	62 %	66 %	63 %
Dx(I) = Dy(I) (s^{-1})	$<4{\cdot}10^6$								$<4{\cdot}10^6$							
Dz(I) 10^{-9} (± 5 %) (s^{-1})	2.2	1.5	1.4	2.0	4.2	3.4	3.2	3.3	3.1	1.5	2.0	2.9	3.0	3.2	3.3	3.1
β(I) ± 0.5 (°)	37	37	37	38	38	38	38	39	34	36	36	36	36	36	37	37
γ(I) ± 0.5 (°)	57	60	59	55	64	65	66	60	90	90	90	90	90	90	90	90
Type II																
N(II) ± 2 %	59 %	58 %	59 %	54 %	48 %	48 %	45 %	46 %	41 %	42 %	43 %	45 %	41 %	38 %	34 %	37 %
Dx(II) = Dy(II) (s^{-1})	$<4{\cdot}10^6$								$<4{\cdot}10^6$							
Dz(II) 10^{-8} (±5 %) (s^{-1})	2.7	2.8	2.8	3.6	4.4	4.9	5.4	6.5	1.9	2.0	2.3	2.3	2.4	2.6	3.1	2.9
β(II) ± 0.5 (°)	51	51	51	50	48	47	47	47	61	56	59	59	56	55	55	55
γ(II) ± 0.5 (°)	90	90	90	90	90	90	90	90	90	90	90	90	90	90	90	90

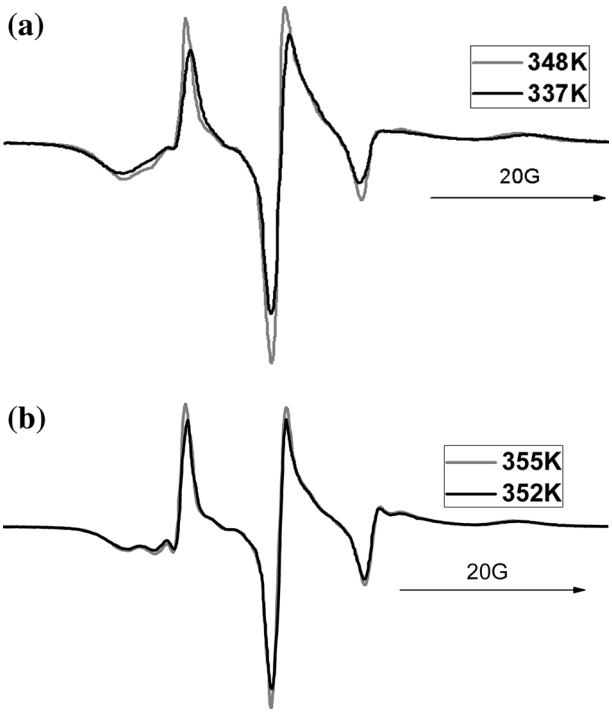

Fig. 5 EPR spectra of radical C4 in SmC phase (**a**) and SmA phase (**b**) of HOPDOB

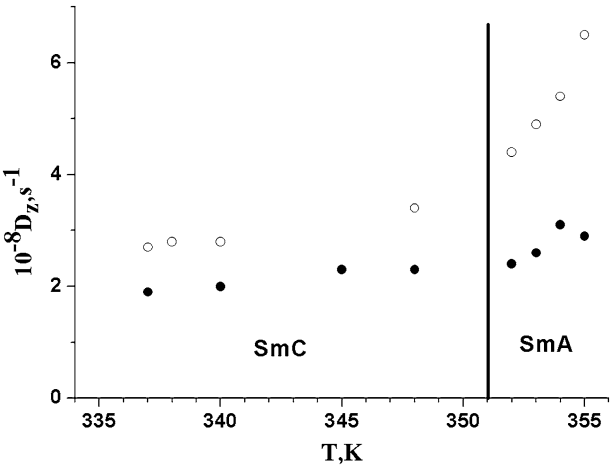

Fig. 6 Temperature dependence of rotation diffusion coefficients for type II radicals C4 (*open circles*) and C15 (*closed circles*) in matrix of HOPDOB. *Line* corresponds to the temperature of SmC–SmA transition

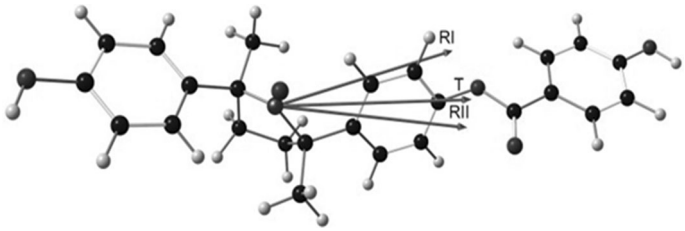

Fig. 7 Rotational axes of radicals of type I (RI) and type II (RII) and the main inertia axis (*T*) of central fragment of paramagnetic molecules

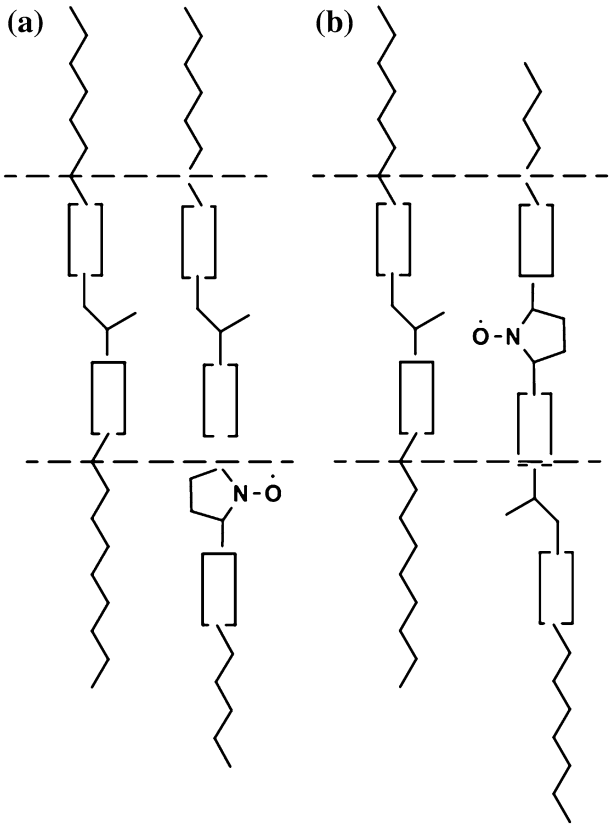

Fig. 8 Hypothetical structure of two modes of localization of the probe molecules in the smectic media

medium. The possible modes of localization are shown in Fig. 8. Zigzags represent the long alkyl substitutes, rectangles stand for the benzene rings, the ester groups are marked by bent lines between the rectangles, pentagon stands for pyrrolidine. Two ways of localization (Fig. 8a, b) differ by position of probe molecule relative to smectic layer.

Regardless of cause, probe molecules in one localization are strongly incorporated in the layer of smectic than other one. Thus, the different rotational properties of radicals in these two localizations reflect the difference of local conditions in positions in structure of smectic layer.

4 Conclusions

Molecules of spin probes can be localized in smectic matrices by one or several modes. The spin probes studied at present work demonstrate unique localization in matrix of 8CB but have dual localization in HOPOOB and HOPDOB. Radicals with different localization are characterized by sufficiently different coefficients of rotation diffusion as well as directions of rotational axes in the molecular frame. Spin probe technique can be used for investigation of the spatial variation of properties in smectic media.

Acknowledgments This work was supported by the Russian Foundation for Basic Research under Grants No. 14-03-00323 and 14-02-31882. Some numerical calculations were performed with the use of Chebyshev Supercomputer at Moscow University.

References

1. J. Michl, E.W. Thulstrup, *Spectroscopy with Polarized Light: Solute Alignment by Photoselection in Liquid Crystals, Polymers and Membranes* (Weinheim; New York: VCH Publishers; 1986)
2. L.L. Chapoy, D.B. DuPre, J. Chem. Phys. 70, 2550–2553 (1979)
3. J.M. Daniels, P.E. Cladis, P.L. Finn, L.S. Powers, J.C. Smith, R.W. Filas, J.W. Goodby, T.M. Leslie, J. Appl. Phys. **53**, 6127–6136 (1982)
4. V.G. Chigrinov, V.M. Kozenkov, H.-S. Kwok, *A Photoalignment of Liquid Crystalline Materials: Physics and Applications* (Wiley, Chichester, 2008)
5. D. Dauman, E. Chrzumnicka, E. Wolarz, Mol. Cryst. Liq. Cryst. **352**, 67–76 (2000)
6. E. Wolarz, D. Bauman, J. Polym. Sci., Part B: Polym. Phys. **31**, 383–387 (1993)
7. E. Wolarz, E. Chrzumnicka, T. Fischer, J. Stumpe, Dyes Pigm. **75**, 753–760 (2007)
8. T.S. Yankova, N.A. Chumakova, D.A. Pomogailo, A.Kh. Vorobiev, Liq. Cryst. **40**, 1135–1145 (2013)
9. T.S. Yankova, A.Yu. Bobrovsky, A.Kh. Vorobiev, J. Phys. Chem. B. 116, 6010–6016 (2012)
10. G. Luckhurst, R.N. Yeates, J. Chem. Soc., Faraday Trans. **2**(72), 996–1009 (1976)
11. J.H. Freed, in *Spin Labeling: Theory and Applications*, ed. by L.J. Berliner (Plenum Press, New York, 1976), p. 53
12. D.J. Schneider, J.H. Freed, in *Biological Magnetic Resonance*, vol. 8, ed. by L.J. Berliner, J. Reuben (Plenum, New York, 1989), p. 1
13. A.Kh. Vorobiev, N.A. Chumakova, in *Simulation of Rigid-Limit and Slow-Motional EPR Spectra for Extraction of Quantitative Dynamic and Orientational Information*, ed. by A.I. Kokorin. Nitroxides—Theory, Experiment and Applications (Intech, Rijeka, 2012)
14. C.F. Polnaszek, J.H. Freed, J. Phys. Chem. **79**, 2283–2306 (1975)
15. Y.C. Kim, S.H. Lee, J.L. West, E. Gelerinter, J. Appl. Phys. **77**, 1914–1922 (1995)
16. M. Ge, J.H. Freed, Biophys. J. **85**, 4023–4040 (2003)
17. Z. Liang, Y. Lou, J.H. Freed, L. Columbus, W.L. Hubbell, J. Phys. Chem. B **108**, 17649–17659 (2004)
18. P.J. Le Masurier, G.R. Luckhurst, J. Chem. Soc., Faraday Trans. **94**, 1593–1601 (1998)
19. E. Melrovitch, J.H. Freed, J. Phys. Chem. **84**, 2459–2472 (1980)
20. H. Gopee, A.N. Cammidge, V.S. Oganesyan, Angew. Chem. Int. Ed. **52**, 8917–8920 (2013)

21. N.A. Chumakova, D.A. Pomogailo, T.S. Yankova, A.Kh. Vorobiev, Mol. Cryst. Liq. Cryst. **540**, 196–204 (2011)
22. O.H. Griffith., P.C. Jost, in *Spin Labeling: Theory and Applications*, ed. by L.J. Berliner (Plenum Press, New York, 1976), p. 454
23. D.E. Budil, L. Sanghyuk, S. Saxena, J.H. Freed, J. Magn. Reson., Ser A. 120, 155–189 (1996)
24. A.Kh. Vorobiev, T.S. Yankova, N.A. Chumakova, J Chem. Phys. **409**, 61–73 (2012)
25. D.S. Hulme, E.P. Raynes, K.J. Harrison, J. Chem. Soc. Chem. Comm. **1974**, 98–99
26. L.A. Beresnev, L.M. Blinov, V.A. Baikalov, E.P. Pozhidaev, G.V. Purvanetskas, A.I. Pavluchenko, Mol. Cryst. Liq. Cryst. **89**, 327–338 (1982)
27. V. Vill, *LiqCryst 5.0—Database of Liquid Crystalline Compounds* (LCI Publisher, Hamburg, 2010); liqcryst.lci-publisher.com
28. S. Petrov, P. Simova, Cryst. Res. Technol. **21**, 959–965 (1986)
29. T.T. Blair, M.E. Neubert, M. Tsai, C-C. Tsai, J. Phys. Chem. Ref. Data. **20**, 189–204(1991)
30. S. Pestov, V. Vill, in *Liquid Crystalline Substances*, ed. by W. Martienssen. Springer Handbook of Condensed Matter and Materials Data (Springer, Berlin, 2005), pp. 941–977
31. N. Ikuma, R. Tamura, S. Shimono, N. Kawame, O. Tamada, N. Sakai, J. Yamauchi, Y. Yamamoto, Angew. Chem. Int. Ed. **43**, 3677–3682 (2004)
32. N. Ikuma, R. Tamura, S. Shimono, Y. Uchida, K. Masaki, J. Yamauchi, Y. Aoki, H. Nohira. Adv. Mater. **18**, 477–480 (2006)
33. http://www.chem.msu.ru/eng/lab/chemkin/ODF3/
34. B. Dzikovski, D. Tipikin, V. Livshits, K. Earle, J. Freed. Phys. Chem. Chem. Phys. **11**, 6676–6688 (2009)
35. J. Pilař, J. Labskỳ, J. Kálal, J.H. Freed, J. Phys. Chem. **83**, 1907–1914 (1979)
36. J.E. Dennis., D.M. Gay, R.E. Welsch, ACM Transactions on Mathematical Software **7**, 348–368 (1961)
37. M.A. Gunina., N.S. Kucherepa, SM. Pestov., LG. Kuz'mina, Crystallography Reports. **57**, 524-527 (2012)
38. L.G. Kuz'mina, II. Konstantinov, E.Kh. Lermontova, Mol. Cryst. Liq. Cryst. **588**, 1–8 (2014)